Inorganic Chemistry
Cite This: Inorg. Chem. 2018, 57, 1298−1310
Article
pubs.acs.org/IC

Excited-State Processes of Cyclometalated Platinum(II) Charge-Transfer Dimers Bridged by Hydroxypyridines

Arnab Chakraborty, James E. Yarnell, Roger D. Sommer, Subhangi Roy, and Felix N. Castellano*

Department of Chemistry, North Carolina State University, Raleigh, North Carolina 27695-8204, United States

Supporting Information

ABSTRACT: A series of four anti-disposed dinuclear platinum(II) complexes featuring metal−metal-to-ligand charge-transfer (MMLCT) excited states, bridged by either 2-hydroxy-6-methylpyridine or 2-hydroxy-6-phenylpyridine and cyclometalated with 7,8-benzoquinoline or 2-phenylpyridine, are presented. The 2-hydroxypyridine bridging ligands control intramolecular d^8−d^8 metal−metal σ interactions, affecting the frontier orbitals' electronic structure, resulting in marked changes to the ground- and excited-state properties of these complexes. Three of these molecules possess reversible one-electron oxidations in cyclic voltammetry experiments as a result of strong intramolecular metallophilic interactions. In this series of molecules, X-ray crystallography revealed Pt−Pt distances ranging between 2.815 and 2.878 Å; the former represents the shortest reported metal−metal distance for platinum(II) dimers possessing low-energy MMLCT transitions. All four molecules reported here display visible absorption bands beyond 500 nm and feature MMLCT-based red photoluminescence (PL) above 700 nm at room temperature with high PL quantum yields (up to 4%) and long excited-state lifetimes (up to 341 ns). The latter were recorded using both transient PL and transient absorption experiments that self-consistently yielded quantitatively identical excited-state lifetimes. The energy-gap law was successfully applied to this series of chromophores, documenting this behavior for the first time in molecules possessing MMLCT excited states. The combined data illustrate that entirely new classes of MMLCT chromophores can be envisioned using bridging pyridyl hydroxides in cooperation with various C^N cyclometalates to achieve photophysical properties suitable for excited-state electron- and energy-transfer chemistry.

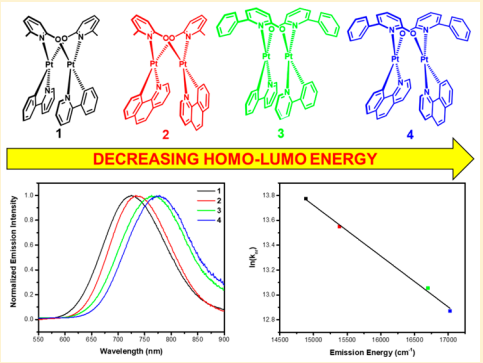

INTRODUCTION

Square-planar transition-metal complexes have recently experienced an increase in research interest, particularly those based on platinum(II). Many of these molecules possess notable photophysical properties, making them useful in applications including optoelectronic devices,[1−5] photocatalysis,[6−9] cation sensing,[10,11] pH sensing,[12,13] and cyanogen halide detection,[14] among others.[15−19] The platinum(II) complexes used in many of these research fields are based on a mononuclear structure containing an aromatic π-accepting chelating ligand, such as 1,10-phenanthroline or 2,2′-bipyridine, along with other supporting ancillary ligands. The lowest-energy excited state in these types of chromophores can vary but generally is LC mixed with some fraction of charge-transfer character that is metal-to-ligand (MLCT) and/or ligand-to-ligand (LLCT) charge transfer in nature. In addition, platinum(II) complexes benefit from large d-orbital splitting, rendering the metal-centered (MC) states too high in energy to effectively deactivate the excited state, resulting in complexes that can be highly emissive at room temperature. This effect is more pronounced when cyclometalating ligands are used because of their strong σ-donating character at the cyclometalating carbon. The strong ligand field provided by the aromatic N^C ligand(s) and additional π donation from the metal into this ligand(s) renders these cyclometalated complexes extremely stable.

Square-planar platinum(II) complexes are also known to exhibit strong metal−metal interactions in the solid state and are responsible for the range of colors characteristic of these solids. Their propensity to engage in such intermolecular metallophilic interactions forming extended topologies in the solid state has been thoroughly investigated.[20−22] Through the use of select bridging ligands and appropriate chelates, soluble dinuclear platinum(II) complexes can be constructed to mimic the metal−metal interactions observed in the solid state. In essence, positioning the two metal centers close together enables d_{z^2}−d_{z^2} orbital overlap, resulting in the formation of dσ and dσ* orbitals. This gives rise to characteristic metal−metal-to-ligand charge-transfer (MMLCT) transitions (Figure 1) at lower energy with respect to the analogous mononuclear complex. Because the degree of d_{z^2} overlap largely determines the relative splitting between the dσ and dσ* orbitals, the energy of the dσ* → π* MMLCT transition depends strongly on the metal−metal distance, and thus the transition energy decreases as the metal centers coalesce. The most extensively

Received: October 25, 2017
Published: January 16, 2018

DOI: 10.1021/acs.inorgchem.7b02736
Inorg. Chem. 2018, 57, 1298−1310

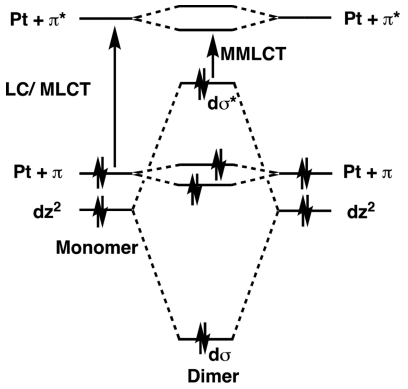

Figure 1. Simplified molecular orbital diagram illustrating d^8–d^8 interactions in platinum(II) dimers featuring MMLCT excited states.

studied dinuclear platinum(II) transition-metal complex is arguably the phosphite-bridged species $[Pt_2(P_2O_5)_4H_8]^{4-}$, commonly termed "platinum POP" and abbreviated as $[Pt_2(POP)_4]^{4-}$. Gray and co-workers have extensively investigated the spectroscopic and redox properties of this d^8–d^8 dimer.[23−26] Evidence for strong Pt−Pt interactions in the excited state in $[Pt_2(POP)_4]^{4-}$ was established by static and time-resolved absorption, photoluminescence (PL), and resonance Raman spectroscopy.[23−27] Several recent pump−probe X-ray scattering and absorption experiments conducted on the benchmark $[Pt_2(POP)_4]^{4-}$ complex reveal a Pt−Pt contraction of 0.24−0.31 Å following $d\sigma^* \rightarrow p\sigma$ excitation, formally depopulating the $d\sigma^*$ orbital in the excited state.[28−30] Another variant of this structure has only recently appeared,[31−34] illustrating the limited parameter space available for tuning excited-state behavior when the optical transitions are exclusively derived from metal-based molecular orbitals.[26] There have also been numerous studies related to platinum(II) MLCT excited states featuring metal−metal interactions in both the solid state and fluid solutions.[35−43]

Previous reports by Thompson and co-workers on platinum(II) dimers containing the 2-(2,4-difluorophenyl)-pyridyl N^C cyclometalating ligand showed that the photophysical behavior of these chromophores can be systematically tuned by introducing steric bulk in the 3 and 5 positions of the bridging pyrazolates.[44] In essence, these pyrazolate substitutions modulated the Pt−Pt distances in a predictable manner, revealing systematic tuning of both the absorption and PL properties. In a subsequent study, this same class of molecules was successfully applied as phosphorescent dopants in organic light-emitting diodes.[45] Our group and others have further expanded this research area by synthesizing new pyrazolate-bridged dimers with numerous cyclometalating ligands.[40,46−52] The Ma group recently dubbed these complexes "molecular butterflies", consistent with their geometric shape and cooperative flapping motion generated upon visible-light excitation.[51,52] These molecules have been extensively studied with a battery of techniques including conventional and ultrafast transient absorption spectroscopy, X-ray transient absorption spectroscopy, transient absorption anisotropy, and time-resolved wide-angle X-ray scattering. The collective combination of these investigations has detailed the structural changes of these types of molecules produced upon light excitation.[53−56]

When pyridine-2-thiolate ions (i.e., 2-mercaptopyridine) were used in concert with 2-phenylpyridine (ppy)-supported platinum(II) centers, the shortest Pt−Pt distance was recorded for the MMLCT genre of chromophores in 2004, 2.8491(4) Å.[57−62] The poor solubility of this red-emitting complex along with its sensitivity toward halogenated solvents, readily undergoing dark oxidative addition chemistry resulting in the formation of nonemissive platinum(III) species, limited more extensive photophysical investigations.[57] If alternate bridging ligands could be identified to accommodate more intimate Pt−Pt interactions while circumventing undesired oxidative addition chemistry, MMLCT-based photochemistry and photophysics could markedly expand beyond the current inventory of available chromophores.

The objective of the present study was to generate strong metal−metal interactions between two platinum centers by incorporating new bridging ligands into the classic A-frame geometry, retaining low-energy MMLCT excited states. Our methodology simply posed the question of whether the substitution of −OH for −SH in 2-mercaptopyridine-like structures would enable such a platform for the creation of new molecules. Here we report the synthesis, electrochemistry, and photophysical characterization of a new series of four platinum(II) dimers utilizing both 2-hydroxy-6-methylpyridine (MePyO) and 2-hydroxy-6-phenylpyridine (PhPyO) as bridging ligands for the first time along with ppy and 7,8-benzoquinoline (bzq) cyclometalating ligands (**1**−**4**; Figure 2). We observed that unlike the 2-mercaptopyridine-bridged (N^S) platinum(II) dimers, these related N^O-bridged molecules are both thermally and photochemically stable and not susceptible to oxidative addition in halogenated solvents. In addition, they feature high solubility in both coordinating and noncoordinating solvents (between 5 and 10 mM), making these molecules easy to study and valuable for both fundamental investigations and emerging applications. Unlike the benchmark pyrazolate dimers, the N^O-bridged complexes reported in this study were all isolated exclusively as their anti

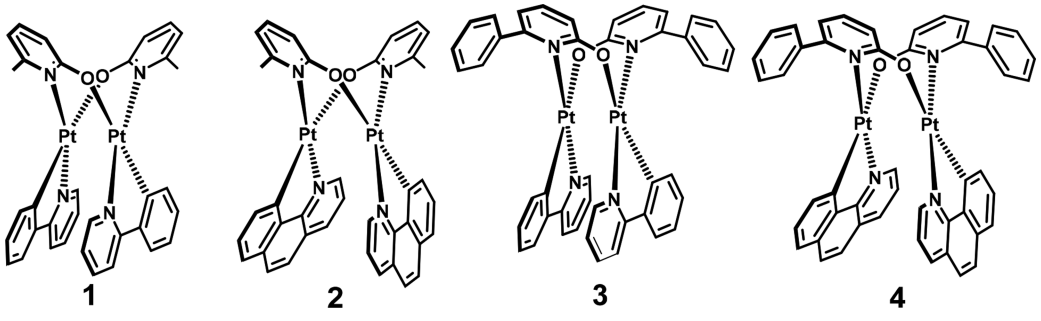

Figure 2. Structures of the 2-hydroxypyridyl-bridged dinuclear platinum(II) complexes.

DOI: 10.1021/acs.inorgchem.7b02736
Inorg. Chem. 2018, 57, 1298−1310

Scheme 1. Generalized Synthetic Scheme for the N^O-Bridged Dinuclear Platinum(II) Complexes[a]

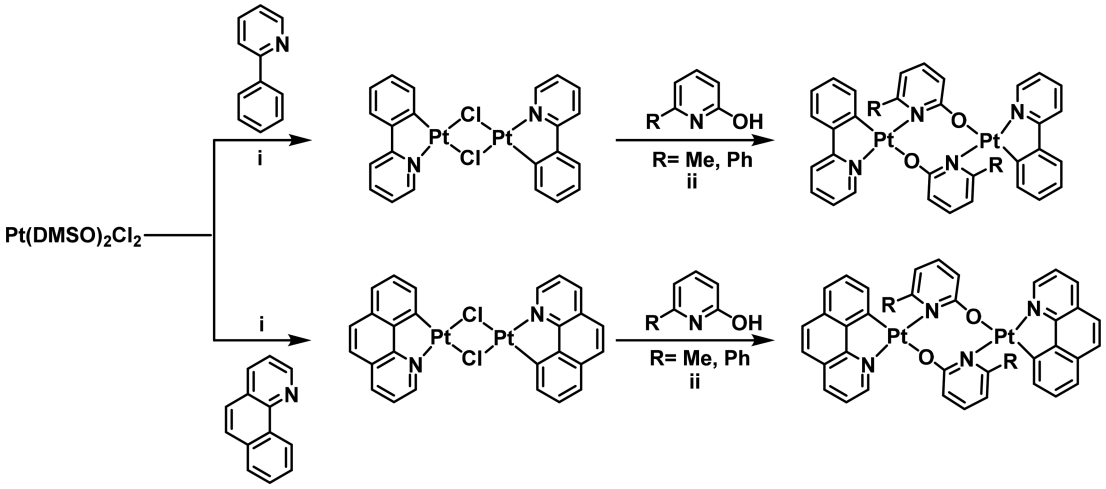

[a]Reagents and conditions: (i) 2-ethoxyethanol/water refluxed overnight. (ii) K_2CO_3 and 1,2-dichloroethane refluxed at 88 °C for 1 day.

isomers (trans with respect to the relative orientation of the two N^C and two N^O ligands), confirmed through X-ray crystallography and ^{1}H NMR spectroscopy. Selective formation of the anti stereoisomer is consistent with that described by Kato and co-workers in related 2-mercaptopyridine-bridged platinum(II) dimers and likely results from the strong trans-directing nature of the carbanion portion of the ppy and bzq cyclometalating ligands.[57−61] All of the new complexes reported here display visible absorption bands beyond 500 nm and feature MMLCT-based red PL above 700 nm at room temperature with high PL quantum yields (up to 4%) and long excited-state lifetimes (up to 341 ns). The latter were recorded using both transient PL and absorption experiments that self-consistently yielded quantitatively identical excited-state lifetimes. The energy-gap law was successfully applied to this series of chromophores, documenting this behavior for the first time in molecules possessing MMLCT excited states. Finally, [Pt(bzq)(μ-MepyO)]$_2$ (**2**) was shown to possess the closest Pt−Pt distance [2.8155(3) Å] reported for a MMLCT complex to date. The combined data illustrate that entirely new classes of MMLCT chromophores can be envisioned using bridging pyridyl hydroxides in cooperation with various C^N cyclometalates to achieve photophysical properties suitable for excited-state electron- and energy-transfer chemistry.

EXPERIMENTAL SECTION

Reagents and Chemicals. All synthetic manipulations were performed under an inert dry nitrogen atmosphere using standard techniques. All reagents were purchased from VWR and used as received. The precursor Pt(DMSO)$_2$Cl$_2$ and the intermediate cyclometalated dichloro-bridged platinum(II) dimers [Pt(ppy)(μ-Cl)]$_2$ and [Pt(bzq)(μ-Cl)]$_2$ were synthesized according to their published procedures.[46,63,64] Spectroscopic samples were prepared using spectroscopic-grade tetrahydrofuran (THF) and degassed using the freeze−pump−thaw technique.[65]

Synthesis of the [Pt(N^C)(μ-N^O)]$_2$ Complexes. A generalized procedure for the synthesis of 2-hydroxypyridyl-bridged dimers is presented in Scheme 1; full details are provided as Supporting Information. Briefly, the intermediate dichloride-bridged dinuclear platinum(II) complex was dissolved in 30 mL of 1,2-dichloroethane, and 2 equiv of the respective 2-hydroxypyridyl ligand was added, followed by the addition of a large excess of K_2CO_3. The reaction mixture was refluxed under N_2 at 88 °C for 1 day. The excess unreacted K_2CO_3 was filtered out, and the resulting solution was evaporated to dryness. The solid obtained was washed several times with acetonitrile, filtered, and dried under vacuum. The dimers were isolated exclusively as the anti isomer in all instances.

*anti-[Pt(ppy)(μ-MepyO)]$_2$ (**1**).* Yield: 57% (222 mg). ^{1}H NMR (400 MHz, CD_2Cl_2, ppm): 8.32 (d, J = 5.8 Hz, 2H), 7.40 (t, J = 7.8 Hz, 2H), 7.25 (t, J = 7.7 Hz, 2H), 7.11 (d, J = 8.1 Hz, 2H), 6.95 (d, J = 7.7 Hz, 2H), 6.87 (t, J = 7.3 Hz, 2H), 6.80 (t, J = 7.3 Hz, 2H), 6.48 (d, J = 8.7 Hz, 2H), 6.38 (d, J = 6.8 Hz, 2H), 6.29 (t, J = 6.0 Hz, 2H), 6.23 (d, J = 7.6 Hz, 2H), 2.80 (s, 6H). ESI-HRMS. Found: m/z 913.1505 (MH^+). Calcd for $C_{34}H_{29}N_4O_2{}^{194}Pt_2$: m/z 913.1544. Anal. Calcd (found) for $C_{34}H_{28}N_4O_2Pt_2{\cdot}CH_3CN$: C, 45.24 (45.27); H, 3.27 (3.22); N, 7.33 (7.19).

*anti-[Pt(bzq)(μ-MepyO)]$_2$ (**2**).* Yield: 50% (188 mg). ^{1}H NMR (400 MHz, CD_2Cl_2, ppm): 8.09 (dd, J = 5.4 and 1.3 Hz, 2H), 7.36 (m, 8H), 7.18 (t, J = 7.3 Hz, 2H), 7.04 (d, J = 8.7 Hz, 2H), 6.59 (d, J = 9.2 Hz, 2H), 6.48 (d, J = 7.0 Hz, 2H), 6.45 (d, J = 7.3 Hz, 2H), 6.22 (dd, J = 8.0 and 5.4 Hz, 2H), 2.90 (s, 6H). ESI-HRMS. Found: m/z 961.1504 (MH^+). Calcd for $C_{38}H_{29}N_4O_2{}^{194}Pt_2$: m/z 961.1544. Anal. Calcd (found) for $C_{38}H_{28}N_4O_2Pt_2{\cdot}2.5H_2O$: C, 45.29 (45.36); H, 3.30 (3.38); N, 5.56 (5.36).

*anti-[Pt(ppy)(μ-PhpyO)]$_2$ (**3**).* Yield: 36% (99 mg). ^{1}H NMR (400 MHz, CD_2Cl_2, ppm): 8.18 (d, J = 6.6 Hz, 2H), 7.85 (d, J = 7.5 Hz, 4H), 7.49 (dd, J = 8.6 and 7.0 Hz, 2H), 7.28 (bm, 8H), 6.95 (d, J = 7.7 Hz, 2H), 6.78 (bm, 8H), 6.58 (d, J = 7.7 Hz, 2H), 6.25 (d, J = 7.7 Hz, 2H), 6.15 (t, J = 7.3 Hz, 2H). ESI-HRMS. Found: m/z 1037.1809 (MH^+). Calcd for $C_{44}H_{33}N_4O_2{}^{194}Pt_2$: m/z 1037.1857. Anal. Calcd (found) for $C_{44}H_{32}N_4O_2Pt_2$: C, 50.87 (50.99); H, 3.10 (3.12); N, 5.39 (5.32).

*anti-[Pt(bzq)(μ-PhpyO)]$_2$ (**4**).* Yield: 64% (185 mg). ^{1}H NMR (400 MHz, CD_2Cl_2, ppm): 7.99 (dd, J = 5.4 and 1.3 Hz, 2H), 7.93 (d, J = 7.0 Hz, 4H), 7.58 (dd, J = 8.6 and 7.0 Hz, 2H), 7.27 (m, 12H), 7.15 (t, J = 7.5 Hz, 2H), 6.92 (dd, J = 8.6 and 1.3 Hz, 2H), 6.89 (d, J = 8.7 Hz, 2H), 6.68 (dd, J = 7.0 and 1.3 Hz, 2H), 6.45 (d, J = 7.2 Hz, 2H), 6.10 (d, J = 8.0 Hz, 2H). ESI-HRMS. Found: m/z 1085.1804 (MH^+). Calcd for $C_{48}H_{33}N_4O_2{}^{194}Pt_2$: m/z 1085.1857. Anal. Calcd (found) for $C_{48}H_{32}N_4O_2Pt_2$: C, 53.04 (52.82); H, 2.97 (3.09); N, 5.15 (5.00).

General Techniques. ^{1}H NMR spectra were recorded on a Varian Innova 400 NMR spectrometer operating at 400 MHz. All chemical shifts were referenced to residual solvent signals, and the splitting patterns are assigned as s (singlet), d (doublet), t (triplet), and m (multiplet). High-resolution electrospray ionization mass spectrometry (ESI-HRMS) was performed at the Michigan State University Mass Spectrometry Facility. Elemental analysis data were measured by Atlantic Microlab, Inc., Norcross, GA. Optical absorption spectra were measured on a Shimadzu UV-3600 spectrometer. Steady-state luminescence spectra were obtained from an Edinburgh FS 920 spectrofluorimeter. Quantum yield measurements were performed on

DOI: 10.1021/acs.inorgchem.7b02736
Inorg. Chem. 2018, 57, 1298−1310

Table 1. X-ray Crystallography Data for 1−4

compound	1·CH_3CN	2·H_2O	3	4
CCDC	1582048	1582049	1582051	1582050
chemical formula	$C_{36}H_{31}N_5O_2Pt_2$	$C_{38}H_{30}N_4O_3Pt_2$	$C_{44}H_{32}N_4O_2Pt_2$	$C_{48}H_{32}N_4O_2Pt_2$
fw	955.83	980.84	1038.91	1086.95
temperature (K)	100(2)	100(2)	104(2) K	100(2)
cryst syst	monoclinic	monoclinic	monoclinic	triclinic
space group	$P2_1/c$	$P2_1/n$	$P2_1/c$	$P\bar{1}$
a (Å)	18.6701(13)	12.2856(13)	16.6639(4)	11.0608(3)
b (Å)	11.3682(4)	16.181(2)	15.6077(4)	12.3248(4)
c (Å)	15.1784(7)	15.9506(17)	13.2221(3)	14.4522(4)
α (deg)	90	90	90	82.3251(16)
β (deg)	104.935(4)	106.843(5)	93.4326(13)	73.2432(16)
γ (deg)	90	90	90	88.7946(16)
V (Å)^3	3112.7(3)	3034.8(6)	3432.70(14)	1869.28(10)
Z	4	4	4	2
D_{calc} (g/cm^3)	2.044	2.147	2.01	1.931
F(000)	1816	1864	1984	1040
θ range (deg)	2.12 to 35.00	1.83 to 30.66	1.79 to 31.51	2.06 to 36.32
reflns collected	81313	94796	83172	140426
no. of data/restr/param	0.0307	0.0501	0.0327	0.0504
R_{int}	13686/9/409	9349/1/434	11422/0/469	18137/0/505
GOF	1.012	1.033	1.037	1.018
R_1 [I > 2σ(I)]	0.0199	0.0221	0.0211	0.0248
wR_2 [I > 2σ(I)]	0.0433	0.0506	0.0495	0.046

degassed samples using $[Ru(bpy)_3](PF_6)_2$ in acetonitrile as a relative standard (λ_{em} 621 nm; Φ_{PL} = 0.095).[66]

X-ray Crystallography. Single crystals of **1** were grown from an acetonitrile solution. Single crystals of the remaining molecules **2**−**4** were grown from dichloromethane/hexane solutions. Selected crystallographic data are presented in Table 1. Single crystals suitable for structure analysis were selected from the bulk samples and mounted on MiTeGen mounts using a minimum of paratone N oil. Data were collected on a Bruker-Nonius X8 Kappa Apex II diffractometer by ω and ϕ scans using Mo Kα radiation (λ = 0.71073 Å). Corrections for Lorentz and polarization effects and absorption were made using *SADABS*.[67] All four structures were solved using direct methods and refined using full-matrix least squares (on F^2) using the *SHELX* software package.[68] All non-hydrogen atoms were refined anisotropically. Hydrogen atoms were added at calculated positions, with coordinates and U_{iso} values allowed to ride on the parent atom. The crystal structures were analyzed, and the associated figures were constructed using the *OLEX2* software package.[69]

Electrochemistry. Cyclic and differential-pulse voltammetry (CV and DPV) were performed using a CH Instruments model 600E series electrochemical workstation having a conventional three-electrode arrangement. The measurements were carried under an inert and dry atmosphere of nitrogen in a glovebox (MBraun). Both oxidation and reduction potentials were recorded in acetonitrile containing 0.1 M tetrabutylammonium hexafluorophosphate ($TBAPF_6$) as the supporting electrolyte. A platinum disk was used as the working electrode, a platinum wire as the counter electrode, and $Ag/AgNO_3$ as the reference electrode. Measurements were executed with a scan rate of 100 mV/s unless otherwise stated, and ferrocenium/ferrocene (Fc^+/Fc) was used as an internal standard [$E_{1/2}(Fc^+/Fc)_{obsd}$ = 0.078 ± 0.005 V].[70]

Nanosecond Transient Absorption Spectroscopy. Nanosecond transient absorption measurements were performed on a LP920 laser flash-photolysis system (Edinburgh Instruments). Briefly, a tunable Vibrant 355 Nd:YAG/OPO system (OPOTEK) was used for pulsed-laser excitation. To collect the transient absorption difference spectra in the visible portion of the spectrum, an iStar ICCD camera (Andor Technologies), controlled by the L900 software program (Edinburgh Instruments), was used. Samples were degassed using the freeze−pump−thaw technique in 1-cm-path-length quartz optical cells. Samples were prepared to have optical densities between 0.3 and 0.5 at the excitation wavelength (λ_{ex} = 520 nm; 3.0 mJ/pulse). All flash-photolysis experiments were performed at room temperature. The reported difference spectra and kinetic data are the average of 50 laser shots. The ground-state absorption spectra were measured before and after each experiment to ensure that there was no sample degradation. The single-wavelength transient kinetic data were evaluated using the fitting routines available in *OriginPro 2016*.

Computational Details. Calculations of **1**−**4** were performed using the *Gaussian 09* software package (revision D.01)[71] and the computational resources of the North Carolina State University High Performance Computing Center. Ground-state geometry optimizations and time-dependent density functional theory (TD-DFT) calculations were performed using the B3LYP functional[72,73] and the def2-TZVP basis set of Alrichs' group,[74] as implemented in *Gaussian 09*. The Stuttgart−Dresden effective core potentials[75] (ECPs) were used to replace the core electrons in platinum for all calculations. This combination of the functional and basis set was used in previously studied pyrazolate-bridged platinum dimers and shown to be the most consistent in treating the various excited states observed in these types of molecules.[55] Frequency calculations were performed on all optimized structures to ensure that no imaginary frequencies were observed. The polarizable continuum model was used to simulate the effects of the THF solvent environment for TD-DFT calculations.[76] The simulated electronic spectra were generated using a Gaussian convolution with a half-bandwidth of 0.2 eV with *GaussView 5.0*.[77]

RESULTS AND DISCUSSION

Syntheses and Structural Characterization. The intermediate cyclometalated dichloride-bridged Pt(N^C) dimers were synthesized using the procedure available in the literature.[46] This involved refluxing $Pt(DMSO)_2Cl_2$ with 2−2.5 equiv of the respective cyclometalating ligand in a mixture of 2-ethoxyethanol and water (3:1) overnight. The isolated chloride-bridged dimers were directly used for the synthesis of target complexes in refluxing dichloroethane. The generalized procedure for the synthesis of 2-hydroxypyridyl-bridged dimers presented in Scheme 1 is demonstrative of the facile nature of this chemistry. In all instances, the molecules were exclusively

DOI: 10.1021/acs.inorgchem.7b02736
Inorg. Chem. 2018, 57, 1298−1310

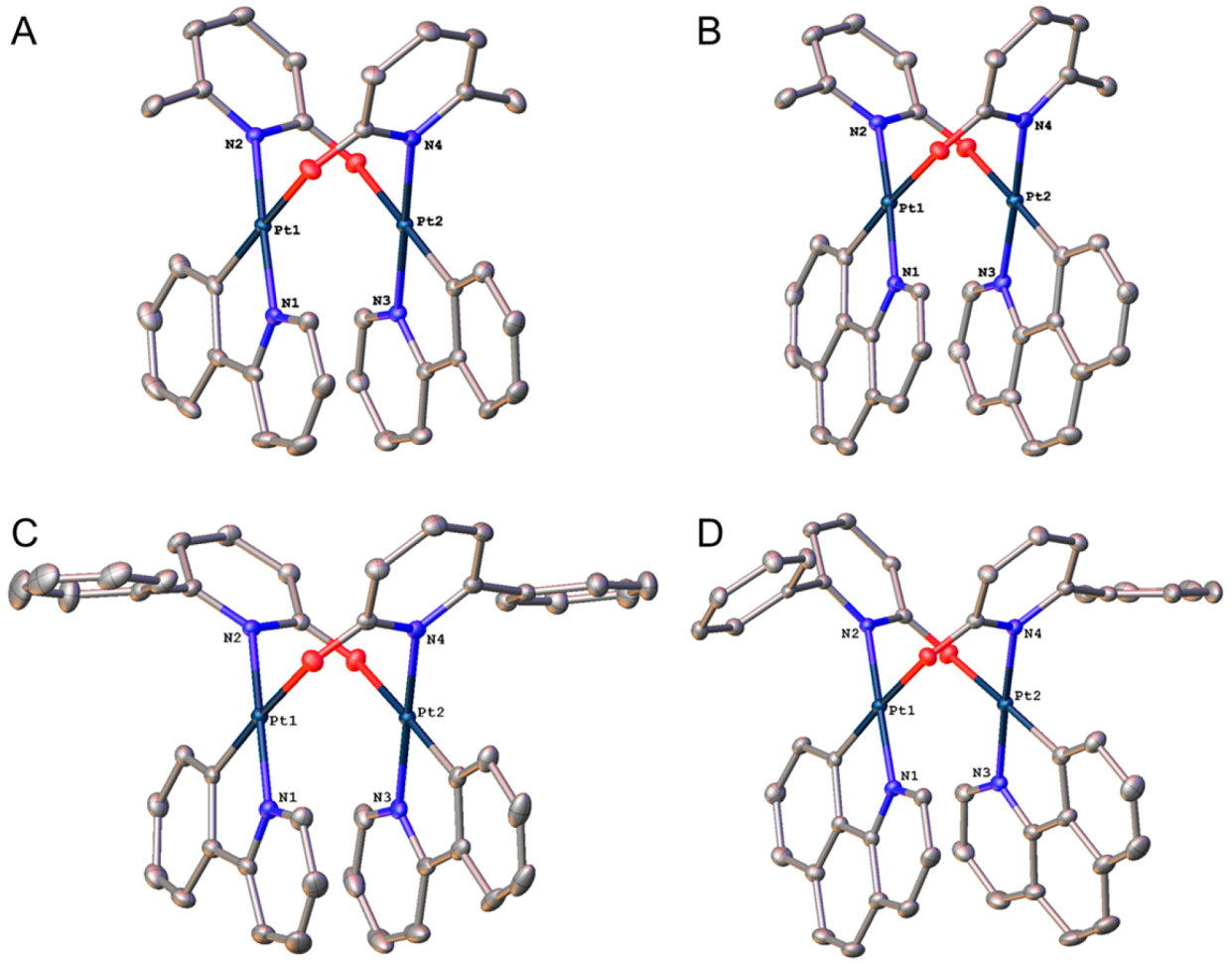

Figure 3. Thermal ellipsoid plots of **1** (A), **2** (B), **3** (C), and **4** (D). Ellipsoids drawn at 50%, with hydrogen atoms removed from structures for clarity.

Table 2. Selected Bond Lengths (Å) and Angles (deg) for 1−4

	1	2	3	4
Pt1−Pt2	2.82413(11)	2.8155(3)	2.87811(14)	2.85745(14)
Pt1−N1	2.0039(17)	2.017(3)	2.009(2)	2.0072(17)
Pt2−N3	2.0172(16)	2.012(2)	2.007(2)	2.0181(18)
Pt1−Pt2−N3	94.07(5)	91.25(7)	91.96(6)	96.31(5)
Pt2−Pt1−N1	91.57(5)	96.87(7)	90.56(6)	92.21(5)
N1−Pt1−Pt2−N3	61.56(5)	61.37(7)	58.15(6)	61.09(5)
Pt1−N2	2.0402(16)	2.041(3)	2.044(2)	2.0355(17)
Pt2−N4	2.0533(16)	2.036(2)	2.036(2)	2.0469(18)
N1−Pt1−N2	176.04(7)	175.79(10)	172.75(9)	176.40(7)
N3−Pt2−N4	176.17(7)	175.86(10)	175.00(9)	175.47(7)

isolated in the anti configuration, as verified by ^{1}H NMR and X-ray crystallography. ESI-HRMS spectra were also consistent with the elemental compositions expected for these newly prepared molecules. Elemental analyses were also consistent with each calculated molecular formula and each determined X-ray crystal structure.

X-ray Crystal Structures. X-ray-quality crystals were obtained for all molecules in this study. The four molecular structures were determined by single-crystal X-ray diffraction, with the data collection and refinement parameters described in the Experimental Section. In general, the four structures have remarkable similarity despite having different bridging and chromophoric ligands attached to the platinum atoms (Figure 3). The Pt−Pt distances, which leads to many unique photophysical properties in the four complexes, are collected in Table 2. The Pt−Pt distance ranged from the largest value observed in **3** with a distance of 2.87811(14) Å to the smallest value measured in **2** of 2.8155(3) Å. The metal−metal distances observed in these complexes are a bit counterintuitive because the increased bulkiness of the bridging ligand (phenyl vs methyl) nominally brings the platinum centers closer together relative to the complexes with respect to those carrying less bulky substituents, as observed in previous platinum(II) pyrazolate structures.[44] Therefore, the smallest Pt−Pt distances would be expected in **3** and **4**, which contain phenyl rings in the 6 position of the pyridine (more bulky)

DOI: 10.1021/acs.inorgchem.7b02736
Inorg. Chem. 2018, 57, 1298−1310

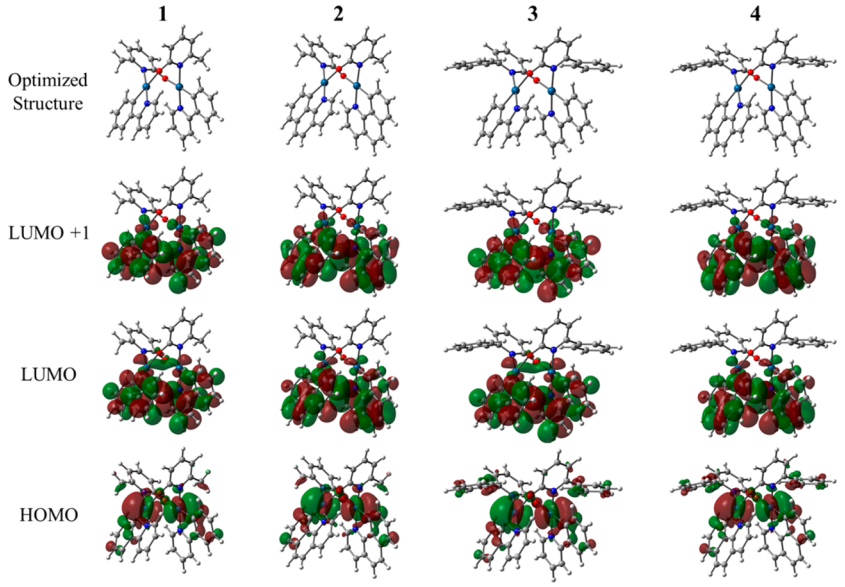

Figure 4. Frontier molecular orbital diagrams constructed for **1**−**4**. Calculations performed at the DFT//B3LYP/Def2-TZVP/SDD level of theory.

relative to 6-methyl groups in **1** and **2** (less bulky). The experimental data reveal that the shortest metal−metal distances are actually observed in **1** and **2**, and this may be due to the relative conformation of the phenyl rings in **3** and **4** and how they influence the crystallization.

Electronic Structure Calculations. DFT and TD-DFT calculations were performed on **1**−**4** to support the ground- and excited-state assignments observed in this study using the B3LYP/Def2-TZVP/SDD level of theory. The B3LYP functional was used because recent studies have demonstrated that it can successfully model the types of excited states observed in platinum complexes similar to the ones in this study.[55,78] The def2-TZVP basis set and SDD ECP combination was used previously by Chen and co-workers to study a similar series of cyclometalated platinum dimers and is shown to be effective at calculating the ground-state structures because the Pt−Pt distances closely match those from the crystal structures.[55] In addition, they were able to show the change of the lowest-energy excited state, LC/MLCT to MMLCT, when the Pt−Pt distance was reduced by the incorporation of bulky substituents on the bridging ligand.

The ground-state structures for **1**−**4** were optimized, and the calculated frontier molecular orbital diagrams are presented in Figure 4. The highest occupied molecular orbital (HOMO), lowest unoccupied molecular orbital (LUMO), and LUMO+1 all look remarkably similar for these complexes, suggesting that the electronic structure does not change significantly across the series. The HOMO mostly resides on the two platinum atoms composed of the antibonding d_{z^2} orbitals, which resemble the dσ* orbital generated by the Pt−Pt σ interaction. LUMO and LUMO+1 are the in-phase and out-of-phase π*-orbital combinations, respectively, localized on the cyclometalating ligand (ppy or bzq).

Electrochemistry. The electrochemical properties of the new molecules were investigated using CV and DPV. In order to provide the appropriate solubility and electrochemical potential window, measurements were conducted in acetonitrile with 0.1 M $TBAPF_6$ as the supporting electrolyte. Peak potentials (E_{pa} or E_{pc}) were recorded with DPV, and the electrochemical reversibility of the dinuclear platinum(II) complexes was examined using CV. The redox potentials for all of the newly synthesized dimers **1**−**4** are presented in Table 3, with all of the requisite cyclic voltammograms and differential-pulse voltammograms provided in Figures S9−S13.

Table 3. Electrochemical Data for 1−4 in CH_3CN with 0.1 M $TBAPF_6$

complex	$E_{1/2}$(ox) (V)	$E_{1/2}$(red) (V)
1	0.0^{ir}	-2.53^{ir}
2	0.0^{r}	-2.35^{ir}
3	-0.11^{r}, 0.31^{ir}	-2.52^{ir}
4	-0.098^{r}, 0.27^{ir}	-2.35^{ir}

Each molecule universally exhibited electrochemically irreversible one-electron reductions in CV experiments. The irreversibility of the reduction process can be attributed to the decreased metal−ligand interaction caused by increased conjugation of the rigidly planar cyclometalating ligands. This is not too surprising because similar observations have been previously reported for various mononuclear and dinuclear cyclometalated platinum(II) complexes.[46,64,79] This precluded any possible characterization of the cyclometalating ligands' spectroelectrochemistry to assist in the transient absorption spectroscopic assignments detailed below. The reduction potentials for the present dimers were in the range of −2.35 to −2.53 V, depending upon the nature of the cyclometalating ligand. It was also observed that there was a decrease in the reduction potential with increasing conjugation in the cyclometalating ligand. This net lowering of the reduction potential is likely due to the increased stabilization of the negative charge on the more delocalized π system. Furthermore, the $E_{1/2}$ values remain completely invariant within each class of cyclometalating ligand and are completely unaffected by the nature of the substitution (methyl vs phenyl) in the bridging moiety. Similar observations have been previously reported for similar classes of platinum(II) dimers.[44,46] These combined data are consistent with the first reduction being localized on one of the cyclometalating ligands in each instance.

DOI: 10.1021/acs.inorgchem.7b02736
Inorg. Chem. 2018, 57, 1298−1310

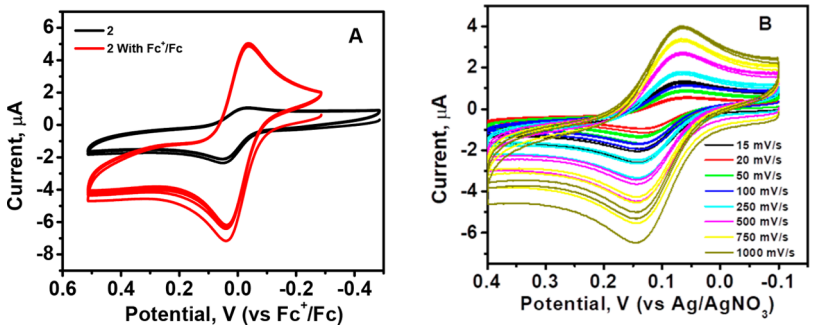

Figure 5. (A) Cyclic voltammogram for the oxidation of **2** in acetonitrile with 0.1 M $TBAPF_6$. A platinum disk was used as the working electrode, a platinum wire as the counter electrode, and $Ag/AgNO_3$ as the reference electrode. (B) Scan rate dependence of the cyclic voltammogram of **2** in acetonitrile with 0.1 M $TBAPF_6$.

Oxidative CV was also performed to evaluate the electrochemical reversibility of the newly synthesized dinuclear complexes, namely, to evaluate the oxidation process that is shared between the two metal centers. An irreversible one-electron oxidation in **1** was revealed, while the remaining complexes exhibited a completely reversible one-electron first oxidation wave. The irreversibility of the first oxidation process in **1** can be attributed to the 16-electron square-planar geometry, making it highly susceptible to nucleophilic attack by CH_3CN on electrochemical time scales, which, in turn, renders the platinum(II) oxidation irreversible.[45,64,80] The presence of a one-electron reversible oxidation in **2**−**4** was further verified by investigating the dependence of the CV response on the scan rate for the oxidation process.[81] A representative example of this reversible electrochemical behavior is presented for **2** in Figure 5. Similar results were obtained for **3** and **4**. These data revealed that ΔE_p remains invariant (75 ± 5 mV) over a wide range of scan rates ranging from 0.015 to 1.75 V/s, as anticipated for a reversible one-electron process. Outside of this window, the oxidation process becomes less reversible, and ΔE_p slowly increased beyond 100 mV. The first oxidation wave in molecules **3** and **4** exhibited a response similar to that of CV scan rate; however, an additional irreversible oxidation wave was documented at more positive applied potentials in these instances. This second wave likely has its origin in the formation of mixed-valence platinum centers that collapse to unknown thermodynamically stable products. Similar multispecies redox electrochemistry from analogous cyclometalated platinum(II) dimers have been previously reported.[58] The first oxidation potentials of these new complexes lie in the order of **1** ≅ **2** > **3** ≅ **4**, demonstrating that, within each class of cyclometalating ligand, the first oxidation process is more facile in the 6-phenylhydroxypyridine-containing species. It appears that the first oxidation potential is also well correlated to increased metal−metal interactions, as suggested by the crystal structures.[46] Overall, the first MC oxidation wave in these molecules is related to the nature of the bridging ligand and therefore the relative energy of the $d\sigma^*$ orbital that modulates with $d_{z^2}-d_{z^2}$ overlap. The measured values for these oxidations are similar to those reported in analogous platinum(II) pyrazolate dimers.[45,46] We note that all attempts at performing oxidative spectroelectrochemistry failed because of decomposition of the one-electron-oxidized species over the time course of the bulk electrolysis experiments. In summary, the first oxidation process appears to be controlled by the nature of the bridging ligands, and the first reduction is dependent on the nature of the N^C cyclometalate installed on the complex.

Electronic Spectroscopy. The electronic spectra of the four molecules in this study are presented in Figure 6 with

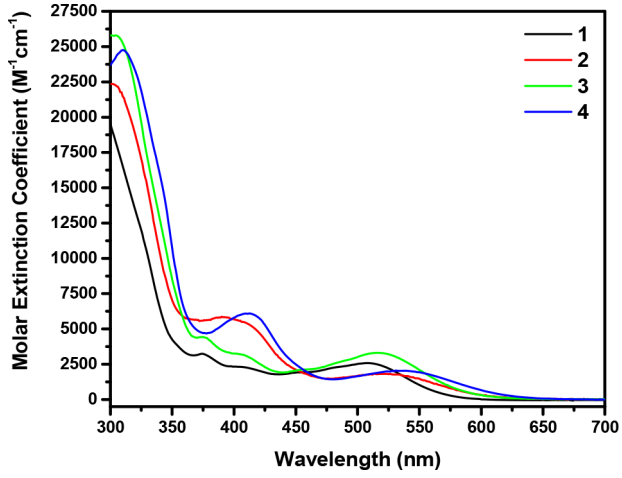

Figure 6. Static electronic spectra of **1** (black), **2** (red), **3** (green), and **4** (blue) in THF.

pertinent experimental data collected in Table 4. As seen in previous platinum dimers with strong metal−metal interactions, the lowest-energy transitions in these chromophores can best be described as MMLCT in character. TD-DFT calculations confirm this assignment because they confirm that the low-energy transition is Pt_2 $d\sigma^* \rightarrow \pi^*$ of the cyclometalating ligand across the series of complexes (Figures S22−S25). These broad and structureless MMLCT bands possess maxima in the visible region ranging from 508 nm (**1**) to 531 nm (**4**), with **2** and **3** falling between at 520 and 516 nm, respectively. The bzq-containing structures (**2** and **4**) both exhibit the lowest-energy MMLCT absorptions with respect to the ppy-carrying chromophores **1** and **3**. The electrochemical energy gaps in these molecules are largely dominated by the N^C ligand reduction potentials and are manifested directly in their electronic spectra. This trend in the excitation energies for the lowest-energy excited state ($S_0 \rightarrow S_1$) is also observed in the TD-DFT calculations. The more intense transitions below 350 nm are assigned as $\pi-\pi^*$ ligand-centered (LC) in character mostly from the cyclometalating subunits, as confirmed by a comparison to the spectra of the uncoordinated ligands. The comparison of the experimental and stimulated electronic spectra for **1**−**4** illustrates that the different optical transitions

DOI: 10.1021/acs.inorgchem.7b02736
Inorg. Chem. 2018, 57, 1298−1310

Table 4. Spectroscopic and Photophysical Properties of 1−4 in THF[a]

complex	λ_{abs}, nm (ε, M^{-1} cm^{-1})[b]	λ_{em} (nm)[b]	Φ_{em} (%)[c]	λ_{em} (nm) at 77 K	τ_{em} (μs) at RT, 77 K	τ_{TA} (ns)	$k_r \times 10^{-4}$ (s^{-1})[d]	$k_{nr} \times 10^{-6}$ (s^{-1})[e]
1	375 (3240), 508 (2580)	726	3.97	685	0.328, 3.59	341	11.6	2.92
2	296 (22300), 390 (5860), 520 (1830)	738	1.88	703	0.216, 2.43	208	9.03	4.80
3	305 (25800), 375 (4430), 516 (3320)	766	0.51	697	0.056, 3.27	55.9	9.12	17.9
4	310 (24800), 413 (6090), 531 (2060)	777	0.33	707	0.040, 2.27	40.3	8.19	24.8

[a]Room-temperature (RT) measurements were performed in THF, and 77 K measurements were performed in MTHF. [b]Absorption and emission maxima, ±2 nm. [c]Quantum yield measurements were performed using deaerated $[Ru(bpy)_3](PF_6)_2$ in acetonitrile as the standard (λ_{em} = 621 nm; Φ_{PL} = 0.095),[66] values ±5%. [d]$k_r = \Phi/\tau$. [e]$k_{nr} = (1 - \Phi)/\tau$.

observed experimentally are modeled well by TD-DFT and support the MMLCT and LC assignments described above (Figure S26).

PL Spectroscopy. The PL spectra of all molecules in this study are presented in Figure 7A. The four chromophores

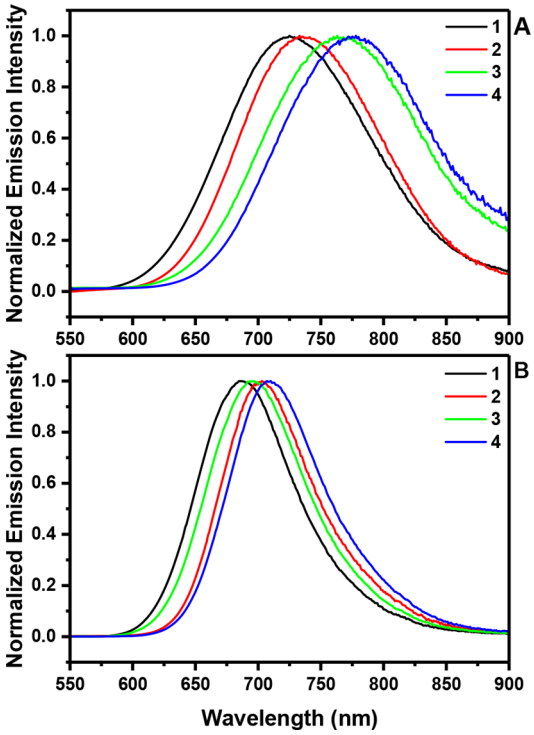

Figure 7. (A) PL spectra of **1** (black line), **2** (red line), **3** (green line), and **4** (blue line) in THF at room temperature. (λ_{ex} = 465 nm). The samples were deaerated using the freeze−pump−thaw method. (B) PL spectra of **1** (black line), **2** (red line), **3** (green line), and **4** (blue line) at 77 K in MTHF glasses (λ_{ex} = 515 nm).

feature a similar broad and featureless emission profile with a fairly large apparent Stokes shift (~6000 cm^{-1}), consistent with the PL radiating from a triplet charge-transfer excited state. The emission maximum red-shifts across the series from 726 nm in **1** to 777 nm in **4**. Unlike the absorption spectra, the PL spectra appear to be sensitive to the nature of the bridging ligand, with the most red-shifted compounds bridged by PhPyO ligands. The only major structure difference relates to the presence of the 6-phenyl substituents on the bridging hydroxypyridine ligands in **3** and **4** that could potentially yield shorter Pt−Pt distances in these chromophores in the excited state at room temperature. Unfortunately, this point remains speculative at present, and we cannot confirm this trend using any straightforward experiment. Upon cooling of the solutions to solid glasses at 77 K in 2-methyltetrahydrofuran (MTHF), the expected rigidochromic blue shift of all molecules was observed; however, the relative energetic ordering across the series changed (Figure 7B). At 77 K, the molecules containing the MePyO bridging ligands (**1** and **2**) blue shift approximately 750 cm^{-1} with respect to room temperature, whereas the PhPyO-bridged dimers (**3** and **4**) are significantly more blue-shifted by ~1275 cm^{-1}. This ultimately results in the ppy cyclometalates having the highest-energy PL at 77 K (**1** and **3**), whereas the complexes containing the bzq ligand (**2** and **4**) have the lowest-energy PL in the series (**1** > **3** > **2** > **4**). This illustrates that the differences in the energies of the 77 K PL are mainly due to the relative π^* energies of the cyclometalating ligands, simply echoing the absorption spectra and electrochemical data, and are not resulting from the nature of the two bridging ligands utilized. This is not surprising because the rigid glass environment markedly restricts the inner-sphere reorganization necessary to bring the two platinum centers closer together after depopulating the dσ^* orbital in the MMLCT transition. The thermally induced Stokes shift observed in each of these molecules is also consistent with the charge-transfer character exhibited by these MMLCT excited states.[82−84]

The single-exponential PL intensity decays of the four molecules were measured in deoxygenated THF at room temperature following pulsed-laser visible-light excitation (λ_{ex} = 465 nm); the combined data are presented in Table 4. The excited-state lifetimes systematically decrease with respect to the ^{3}MMLCT emission maximum, initially suggesting that the energy-gap law (i.e., nonradiative decay) was dictating the excited-state decay in these molecules. Described initially by Jortner and co-workers, the energy-gap law predicts that, for a series of related chromophores with similar electronic excited states, the nonradiative decay rate is largely determined by the vibrational overlap between the ground and excited states.[85,86] Given that the vibrational states of S_0 are generally similar across a series of related chromophores, a smaller energy gap between S_0 and S_1 (or T_1) will result in a larger vibrational overlap between these states, consequentially increasing the nonradiative decay rate constant (k_{nr}).[87] As described by Schanze and co-workers, the simplified relationship between the energy (E_{00}) and the nonradiative rate constant (k_{nr}) can be mathematically related through the use of eq 1a, where E_{00} is the energy between S_0 and S_1 (or T_1), S_m is the Huang−Rhys factor (i.e., the electron−vibration coupling constant), $\hbar\omega_m$ is the average of medium-frequency vibrational modes, and α is the series of terms that are nearly invariant with E_{00}.[82]

$$\ln k_{nr} = \alpha - \ln\left(\frac{\gamma_0}{\hbar\omega_m}\right)E_{00} \quad (1a)$$

DOI: 10.1021/acs.inorgchem.7b02736
Inorg. Chem. 2018, 57, 1298−1310

$$\gamma_0 = \ln\left(\frac{E_{00}}{\hbar\omega_m S_m}\right) - 1 \quad (1b)$$

Using the measured PL quantum yields and the observed single-exponential excited-state lifetimes, radiative (k_r) and nonradiative (k_{nr}) rate constants were calculated for each chromophore (Table 4). Plotting $\ln(k_{nr})$ versus E_{em} revealed a linear relationship (Figure 8), supporting the notion that k_{nr}

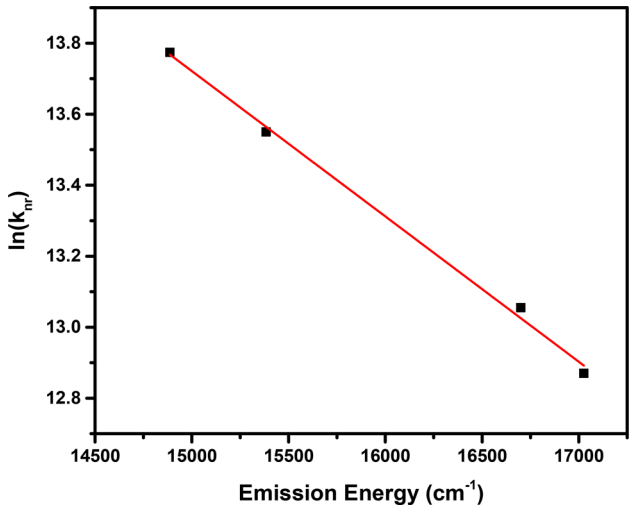

Figure 8. Plot of $\ln(k_{nr})$ versus emission energy for the MMLCT excited states in **1**–**4**.

dominates excited-state decay processes, as seen in many MLCT complexes.[82,87−89] The slope for the line in Figure 8 was found to be -4.1×10^{-4} cm^{-1}, which is significantly smaller than that observed in rhenium(I) and platinum(II) MLCT complexes (slopes of -9.1×10^{-4} and -1.18×10^{-3} cm^{-1}, respectively).[82,88] The slope of this energy-gap relationship is significant because it corresponds to $\gamma_0/\hbar\omega_m$, implying that the acceptor vibrational mode plays a large role in the nonradiative deactivation of the excited state. The acceptor vibrational modes reported in the rhenium(I) and platinum(II) complexes were thought to correspond to diimine C−C ring-stretching vibrations ($\hbar\omega_m \sim 1300$ cm^{-1}), supported by the observation of the vibronic structure in low-temperature emission spectra. In addition, when Schanze and co-workers used 1300 cm^{-1} as the $\hbar\omega_m$ value to simulate the bpy ring-stretching modes, they found good agreement between their calculated and experimental least-squares fit.[82] Because the slope is significantly smaller in the current platinum(II) dimer series, it can be assumed that another acceptor vibrational mode(s) is likely the primary nonradiative deactivation pathway for the excited state. However, using only four related molecules spanning a ∼2000 cm^{-1} emission energy range combined with significant differences in rigidity between the ppy and bzq ligands renders any additional quantitative comparisons too speculative at present.[90] We will note that the ppy ligand is akin to 2,2′-bpy-containing transition-metal complexes, whereas the bzq ligand is structurally related to 1,10-phen-containing molecules.[90] Therefore, **1** and **3** would be expected to exhibit different energy-gap law behaviors with respect to **2** and **4**, which is not the case for the data presented in Figure 8. Fortunately, this can be addressed in the future using one type of N^C acceptor ligand in combination with systematically varied N^O bridging ligands that will undoubtedly facilitate more quantitative comparisons.

Transient Absorption Spectroscopy. The prompt (∼15 ns) excited-state difference spectra for each molecule in this study are presented in Figure 9. The excited-state difference

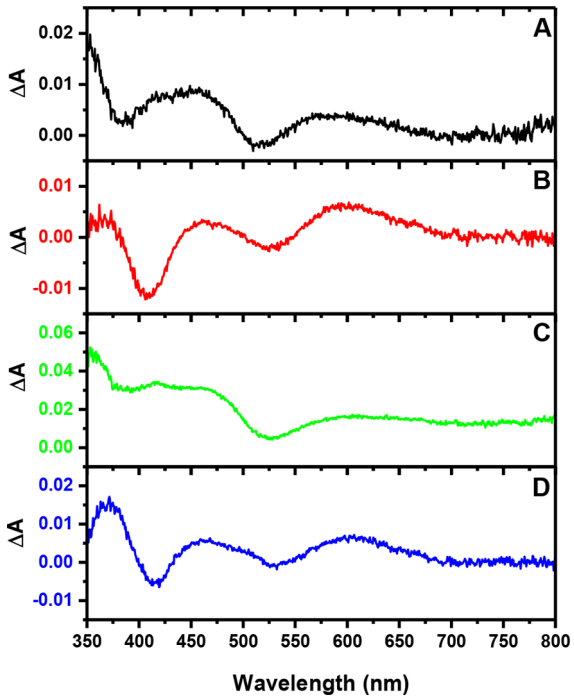

Figure 9. Excited-state absorption difference spectra of **1** (A), **2** (B), **3** (C), and **4** (D) in THF with 520 nm pulsed excitation (3 mJ/pulse, 7 ns fwhm). The samples were deaerated using the freeze−pump−thaw method. Each difference spectrum was measured promptly with a 10 ns gate width.

spectrum for **1** features broad excited-state absorptions at 350, 450, and 575 nm and a weak ground-state bleach located at 510 nm. The decays of these transient features kinetically match each other (and the PL intensity decay experiments) and are all adequately fit to a single-exponential function with a time constant of 341 ns, signifying that the difference spectra are demonstrative of the lowest-energy triplet MMLCT excited state. The excited-state difference spectrum for **2** possesses broad excited-state absorptions at 450 and 575 nm and ground-state bleaches located at 405 and 520 nm. Similar to **1**, the transient features decay with comparable single-exponential time constants (208 ns). The transient absorption features of **3** and **4** are similar to those observed in **1** and **2**, respectively, albeit red-shifted by about 10 nm. Because the π^* chromophoric ligand in **1** and **3** is ppy and that in **2** and **4** is bzq, it is expected that they would have self-consistent transient absorption difference spectra because each radical anion would be localized on either ppy or bzq, generating most of the observed excited-state absorption features. Unfortunately, the irreversibility in the first ligand-localized reduction in both classes of chromophores inhibited quantitative spectroelectrochemistry, and the coincidence of the transient features remains the best mode of comparison. The transient features of **3** and **4** decay with single-exponential time constants of 56 and 40 ns, respectively. The transient absorption kinetics of all four complexes illustrate clear-cut repopulation of the ground state from the lowest-energy excited state and quantitatively match

DOI: 10.1021/acs.inorgchem.7b02736
Inorg. Chem. 2018, 57, 1298−1310

the PL intensity decays measured. Without question, the absorption transients are clearly reporting on the MMLCT-based excited state in each instance, and the signals appear to be sufficient for probing coherence phenomena in these new molecules.

CONCLUSIONS

In summary, four new platinum(II) dimers using ppy and bzq cyclometalates in concert with 6-methyl- or 6-phenyl-substituted 2-hydroxypyridyl bridging ligands were synthesized and thoroughly characterized in terms of structure, electrochemistry, and photophysics. These newly conceived N^O-bridged chromophores are both thermally and photochemically stable and are not susceptible to oxidative addition in halogenated solvents. These N^O-bridged complexes were all isolated exclusively as anti isomers that feature high solubility in both coordinating and noncoordinating solvents, making these molecules valuable for both fundamental investigations and emerging applications. All of these molecules display visible absorption bands beyond 500 nm and MMLCT-based red PL above 700 nm at room temperature with high PL quantum yields and long excited-state lifetimes. The energy-gap law was successfully applied to this series of chromophores, documenting this behavior for the first time in molecules possessing MMLCT excited states. Finally, **2** was shown to have the shortest Pt−Pt distance [2.8155(3) Å] reported for a MMLCT complex to date. This report illustrates that entirely new classes of MMLCT chromophores can be envisioned using bridging pyridyl hydroxides in cooperation with various C^N cyclometalates to achieve photophysical properties suitable for excited-state electron- and energy-transfer chemistry. Because these molecules are able to absorb beyond 500 nm, newly conceived ultrafast laser experiments intended to probe electronic and/or vibrational coherence phenomena in these chromophores can now be realized.

ASSOCIATED CONTENT

Supporting Information

The Supporting Information is available free of charge on the ACS Publications website at DOI: 10.1021/acs.inorgchem.7b02736.

Additional static and time-resolved spectra as well as synthetic details, structural characterization data, electronic structure calculation details, and 3D structures (*XYZ*) of **1**−**4** (PDF)

Accession Codes

CCDC 1582048−1582051 contain the supplementary crystallographic data for this paper. These data can be obtained free of charge via www.ccdc.cam.ac.uk/data_request/cif, or by emailing data_request@ccdc.cam.ac.uk, or by contacting The Cambridge Crystallographic Data Centre, 12 Union Road, Cambridge CB2 1EZ, UK; fax: +44 1223 336033.

AUTHOR INFORMATION

Corresponding Author

*E-mail: fncastel@ncsu.edu.

ORCID

Felix N. Castellano: 0000-0001-7546-8618

Author Contributions

The manuscript was written through contributions of all authors. All authors have given approval to the final version of the manuscript.

Notes

The authors declare no competing financial interest.

ACKNOWLEDGMENTS

We thank the National Science Foundation (Grant CHE-1665033) for support of this research. J.E.Y. was supported by the Air Force Institute of Technology.

REFERENCES

(1) Evans, R. C.; Douglas, P.; Winscom, C. J. Coordination Complexes Exhibiting Room-Temperature Phosphorescence: Evaluation of Their Suitability as Triplet Emitters in Organic Light Emitting Diodes. *Coord. Chem. Rev.* **2006**, *250*, 2093−2126.

(2) Lu, W.; Mi, B.-X.; Chan, M. C. W.; Hui, Z.; Che, C.-M.; Zhu, N.; Lee, S.-T. Light-Emitting Tridentate Cyclometalated Platinum(II) Complexes Containing σ-Alkynyl Auxiliaries: Tuning of Photo- and Electrophosphorescence. *J. Am. Chem. Soc.* **2004**, *126*, 4958−4971.

(3) Wong, W.-Y.; He, Z.; So, S.-K.; Tong, K.-L.; Lin, Z. A Multifunctional Platinum-Based Triplet Emitter for OLED Applications. *Organometallics* **2005**, *24*, 4079−4082.

(4) Ma, B.; Djurovich, P. I.; Yousufuddin, M.; Bau, R.; Thompson, M. E. Phosphorescent Platinum Dyads with Cyclometalated Ligands: Synthesis, Characterization, and Photophysical Studies. *J. Phys. Chem. C* **2008**, *112*, 8022−8031.

(5) McGarrah, J. E.; Kim, Y.-J.; Hissler, M.; Eisenberg, R. Toward a Molecular Photochemical Device: A Triad for Photoinduced Charge Separation Based on a Platinum Diimine Bis(acetylide) Chromophore. *Inorg. Chem.* **2001**, *40*, 4510−4511.

(6) Zhang, D.; Wu, L.-Z.; Zhou, L.; Han, X.; Yang, Q.-Z.; Zhang, L.-P.; Tung, C.-H. Photocatalytic Hydrogen Production from Hantzsch 1,4-Dihydropyridines by Platinum(II) Terpyridyl Complexes in Homogeneous Solution. *J. Am. Chem. Soc.* **2004**, *126*, 3440−3441.

(7) Connick, W. B.; Gray, H. B. Photooxidation of Platinum(II) Diimine Dithiolates. *J. Am. Chem. Soc.* **1997**, *119*, 11620−11627.

(8) Hissler, M.; McGarrah, J. E.; Connick, W. B.; Geiger, D. K.; Cummings, S. D.; Eisenberg, R. Platinum Diimine Complexes: Towards a Molecular Photochemical Device. *Coord. Chem. Rev.* **2000**, *208*, 115−137.

(9) Wang, X.; Goeb, S.; Ji, Z.; Pogulaichenko, N. A.; Castellano, F. N. Homogeneous Photocatalytic Hydrogen Production Using π-Conjugated Platinum(II) Arylacetylide Sensitizers. *Inorg. Chem.* **2011**, *50*, 705−707.

(10) Siu, P. K. M.; Lai, S.-W.; Lu, W.; Zhu, N.; Che, C.-M. A Diiminoplatinum(II) Complex of 4-Ethynylbenzo-15-crown-5 as a Luminescent Sensor for Divalent Metal Ions. *Eur. J. Inorg. Chem.* **2003**, *2003*, 2749−2752.

(11) Lanoë, P.-H.; Fillaut, J.-L.; Toupet, L.; Williams, J. A. G.; Le Bozec, H.; Guerchais, V. Cyclometallated Platinum(II) Complexes Incorporating Ethynyl−Flavone Ligands: Switching between Triplet and Singlet Emission Induced by Selective Binding of Pb^{2+} Ions. *Chem. Commun.* **2008**, 4333−4335.

(12) Wong, K.-H.; Chan, M. C.-W.; Che, C.-M. Modular Cyclometalated Platinum(II) Complexes as Luminescent Molecular Sensors for pH and Hydrophobic Binding Regions. *Chem. - Eur. J.* **1999**, *5*, 2845−2849.

(13) Koo, C.-K.; Ho, Y.-M.; Chow, C.-F.; Lam, M. H.-W.; Lau, T.-C.; Wong, W.-Y. Synthesis and Spectroscopic Studies of Cyclometalated Pt(II) Complexes Containing a Functionalized Cyclometalating Ligand, 2-Phenyl-6-(1*H*-pyrazol-3-yl)-pyridine. *Inorg. Chem.* **2007**, *46*, 3603−3612.

(14) Thomas, S. W.; Venkatesan, K.; Müller, P.; Swager, T. M. Dark-Field Oxidative Addition-Based Chemosensing: New Bis-Cyclo-

DOI: 10.1021/acs.inorgchem.7b02736
Inorg. Chem. 2018, 57, 1298−1310

metalated Pt(II) Complexes and Phosphorescent Detection of Cyanogen Halides. *J. Am. Chem. Soc.* **2006**, *128*, 16641−16648.
(15) Peyratout, C. S.; Aldridge, T. K.; Crites, D. K.; McMillin, D. R. DNA-Binding Studies of a Bifunctional Platinum Complex That Is a Luminescent Intercalator. *Inorg. Chem.* **1995**, *34*, 4484−4489.
(16) Wang, A. H. J.; Nathans, J.; van der Marel, G.; van Boom, J. H.; Rich, A. Molecular Structure of a Double Helical DNA Fragment Intercalator Complex between Deoxy CpG and a Terpyridine Platinum Compound. *Nature* **1978**, *276*, 471−474.
(17) Espinet, P.; Esteruelas, M. A.; Oro, L. A.; Serrano, J. L.; Sola, E. Transition Metal Liquid Crystals: Advanced Materials within the Reach of the Coordination Chemist. *Coord. Chem. Rev.* **1992**, *117*, 215−274.
(18) Ghedini, M.; Pucci, D.; Crispini, A.; Barberio, G. Oxidative Addition to Cyclometalated Azobenzene Platinum(II) Complexes: A Route to Octahedral Liquid Crystalline Materials. *Organometallics* **1999**, *18*, 2116−2124.
(19) Wai-Yin Sun, R.; Ma, D.-L.; Wong, E. L.-M.; Che, C.-M. Some Uses of Transition Metal Complexes as Anti-Cancer and Anti-HIV Agents. *Dalton Trans.* **2007**, 4884−4892.
(20) Miller, J. S.; Epstein, A. J. One-Dimensional Inorganic Complexes. In *Progress in Inorganic Chemistry*; Lippard, S. J., Ed.; John Wiley & Sons, Inc., 1976; pp 1−151.
(21) Schindler, J. W.; Fukuda, R. C.; Adamson, A. W. Photophysics of Aqueous Tetracyanoplatinate(2-). *J. Am. Chem. Soc.* **1982**, *104*, 3596−3600.
(22) Novoa, J. J.; Aullon, G.; Alemany, P.; Alvarez, S. On the Bonding Nature of the M· · ·M Interactions in Dimers of Square-Planar Pt(II) and Rh(I) Complexes. *J. Am. Chem. Soc.* **1995**, *117*, 7169−7171.
(23) Che, C. M.; Butler, L. G.; Gray, H. B. Spectroscopic Properties and Redox Chemistry of the Phosphorescent Excited State of Octahydrotetrakis(phosphorus pentoxide)diplatinate(4-) Ion ($Pt_2(P_2O_5)_4H_8^{4-}$). *J. Am. Chem. Soc.* **1981**, *103*, 7796−7797.
(24) Rice, S. F.; Gray, H. B. Electronic Absorption and Emission Spectra of Binuclear Platinum(II) Complexes. Characterization of the Lowest Singlet and Triplet Excited States of tetrakis(diphosphonato)-diplatinate(4-) Anion ($Pt_2(H_2P_2O_5)_4^{4-}$). *J. Am. Chem. Soc.* **1983**, *105*, 4571−4575.
(25) Che, C. M.; Herbstein, F. H.; Schaefer, W. P.; Marsh, R. E.; Gray, H. B. Binuclear Platinum Diphosphite Complexes. Crystal Structures of Tetrapotassium Bromotetrakis(diphosphito)diplatinate Trihydrate ($K_4[Pt_2(pop)_4Br]\cdot 3H_2O$), a New Linear Chain Semiconductor, and Tetrapotassium Dichlorotetrakis(diphosphito)-diplatinate Dihydrate ($K_4[Pt_2(pop)_4Cl_2]\cdot 2H_2O$). *J. Am. Chem. Soc.* **1983**, *105*, 4604−4607.
(26) Roundhill, D. M.; Gray, H. B.; Che, C. M. Pyrophosphito-Bridged Diplatinum Chemistry. *Acc. Chem. Res.* **1989**, *22*, 55−61.
(27) Striplin, D. R.; Crosby, G. A. Excited States of Homo- and Heteronuclear-Bridged Bimetallic Complexes of Rhodium(I), Iridium-(I), Platinum(II), and Gold(I). Triplet Manifold Splittings, State Assignments, and Symmetry Correlations. *J. Phys. Chem.* **1995**, *99*, 7977−7984.
(28) Novozhilova, I. V.; Volkov, A. V.; Coppens, P. Theoretical Analysis of the Triplet Excited State of the $[Pt_2(H_2P_2O_5)_4]^{4-}$ Ion and Comparison with Time-Resolved X-Ray and Spectroscopic Results. *J. Am. Chem. Soc.* **2003**, *125*, 1079−1087.
(29) van der Veen, R. M.; Milne, C. J.; El Nahhas, A.; Lima, F. A.; Pham, V.-T.; Best, J.; Weinstein, J. A.; Borca, C. N.; Abela, R.; Bressler, C.; et al. Structural Determination of a Photochemically Active Diplatinum Molecule by Time-Resolved EXAFS Spectroscopy. *Angew. Chem., Int. Ed.* **2009**, *48*, 2711−2714.
(30) van der Veen, R. M.; Cannizzo, A.; van Mourik, F.; Vlček, A.; Chergui, M. Vibrational Relaxation and Intersystem Crossing of Binuclear Metal Complexes in Solution. *J. Am. Chem. Soc.* **2011**, *133*, 305−315.
(31) Durrell, A. C.; Keller, G. E.; Lam, Y.-C.; Sýkora, J.; Vlček, A.; Gray, H. B. Structural Control of $^1A_{2u}$-to-$^3A_{2u}$ Intersystem Crossing in Diplatinum(II,II) Complexes. *J. Am. Chem. Soc.* **2012**, *134*, 14201−14207.
(32) Záliš, S.; Lam, Y.-C.; Gray, H. B.; Vlček, A. Spin−Orbit TDDFT Electronic Structure of Diplatinum(II,II) Complexes. *Inorg. Chem.* **2015**, *54*, 3491−3500.
(33) Darnton, T. V.; Hunter, B. M.; Hill, M. G.; Záliš, S.; Vlček, A.; Gray, H. B. Reduced and Superreduced Diplatinum Complexes. *J. Am. Chem. Soc.* **2016**, *138*, 5699−5705.
(34) Gray, H. B.; Záliš, S.; Vlček, A. Electronic Structures and Photophysics of d^8-d^8 Complexes. *Coord. Chem. Rev.* **2017**, *345*, 297−317.
(35) Miskowski, V. M.; Houlding, V. H. Electronic Spectra and Photophysics of Platinum(II) Complexes with α-Diimine Ligands. Solid-State Effects. 1. Monomers and Ligand π Dimers. *Inorg. Chem.* **1989**, *28*, 1529−1533.
(36) Miskowski, V. M.; Houlding, V. H. Electronic Spectra and Photophysics of Platinum(II) Complexes with α-Diimine Ligands Solid-State Effects. 2. Metal-Metal Interaction in Double Salts and Linear Chains. *Inorg. Chem.* **1991**, *30*, 4446−4452.
(37) Bailey, J. A.; Hill, M. G.; Marsh, R. E.; Miskowski, V. M.; Schaefer, W. P.; Gray, H. B. Electronic Spectroscopy of Chloro-(terpyridine)platinum(II). *Inorg. Chem.* **1995**, *34*, 4591−4599.
(38) Connick, W. B.; Marsh, R. E.; Schaefer, W. P.; Gray, H. B. Linear-Chain Structures of Platinum(II) Diimine Complexes. *Inorg. Chem.* **1997**, *36*, 913−922.
(39) Büchner, R.; Cunningham, C. T.; Field, J. S.; Haines, R. J.; McMillin, D. R.; Summerton, G. C. Luminescence Properties of Salts of the $[Pt(4'Ph\text{-}terpy)Cl]^+$ Chromophore: Crystal Structure of the Red Form of $[Pt(4'Ph\text{-}terpy)Cl]BF_4$ (4′Ph-Terpy = 4′-Phenyl-2,2′:6′,2″-Terpyridine). *J. Chem. Soc., Dalton Trans.* **1999**, 711−718.
(40) Lai, S.-W.; Chan, M. C.-W.; Cheung, T.-C.; Peng, S.-M.; Che, C.-M. Probing d^8−d^8 Interactions in Luminescent Mono- and Binuclear Cyclometalated Platinum(II) Complexes of 6-Phenyl-2,2′-Bipyridines. *Inorg. Chem.* **1999**, *38*, 4046−4055.
(41) Yersin, H.; Donges, D.; Humbs, W.; Strasser, J.; Sitters, R.; Glasbeek, M. Organometallic Pt(II) Compounds. A Complementary Study of a Triplet Emitter Based on Optical High-Resolution and Optically Detected Magnetic Resonance Spectroscopy. *Inorg. Chem.* **2002**, *41*, 4915−4922.
(42) Lai, S.-W.; Lam, H.-W.; Lu, W.; Cheung, K.-K.; Che, C.-M. Observation of Low-Energy Metal−Metal-to-Ligand Charge Transfer Absorption and Emission: Electronic Spectroscopy of Cyclometalated Platinum(II) Complexes with Isocyanide Ligands. *Organometallics* **2002**, *21*, 226−234.
(43) Yam, V. W.-W.; Wong, K. M.-C.; Zhu, N. Solvent-Induced Aggregation through Metal···Metal/π···π Interactions: Large Solvatochromism of Luminescent Organoplatinum(II) Terpyridyl Complexes. *J. Am. Chem. Soc.* **2002**, *124*, 6506−6507.
(44) Ma, B.; Li, J.; Djurovich, P. I.; Yousufuddin, M.; Bau, R.; Thompson, M. E. Synthetic Control of Pt···Pt Separation and Photophysics of Binuclear Platinum Complexes. *J. Am. Chem. Soc.* **2005**, *127*, 28−29.
(45) Ma, B.; Djurovich, P. I.; Garon, S.; Alleyne, B.; Thompson, M. E. Platinum Binuclear Complexes as Phosphorescent Dopants for Monochromatic and White Organic Light-Emitting Diodes. *Adv. Funct. Mater.* **2006**, *16*, 2438−2446.
(46) Chakraborty, A.; Deaton, J. C.; Haefele, A.; Castellano, F. N. Charge-Transfer and Ligand-Localized Photophysics in Luminescent Cyclometalated Pyrazolate-Bridged Dinuclear Platinum(II) Complexes. *Organometallics* **2013**, *32*, 3819−3829.
(47) Rachford, A. A.; Castellano, F. N. Thermochromic Absorption and Photoluminescence in $[Pt(ppy)(\mu\text{-}Ph_2pz)]_2$. *Inorg. Chem.* **2009**, *48*, 10865−10867.
(48) McCusker, C. E.; Chakraborty, A.; Castellano, F. N. Excited State Equilibrium Induced Lifetime Extension in a Dinuclear Platinum(II) Complex. *J. Phys. Chem. A* **2014**, *118*, 10391−10399.
(49) Lai, S.-W.; Chan, M. C. W.; Cheung, K.-K.; Peng, S.-M.; Che, C.-M. Synthesis of Organoplatinum Oligomers by Employing N-Donor Bridges with Predesigned Geometry: Structural and Photo-

DOI: 10.1021/acs.inorgchem.7b02736
Inorg. Chem. 2018, 57, 1298−1310

physical Properties of Luminescent Cyclometalated Platinum(II) Macrocycles. *Organometallics* **1999**, *18*, 3991−3997.
(50) Akatsu, S.; Kanematsu, Y.; Kurihara, T.; Sueyoshi, S.; Arikawa, Y.; Onishi, M.; Ishizaka, S.; Kitamura, N.; Nakao, Y.; Sakaki, S.; et al. Syntheses and Luminescent Properties of 3,5-Diphenylpyrazolato-Bridged Heteropolynuclear Platinum Complexes. The Influence of Chloride Ligands on the Emission Energy Revealed by the Systematic Replacement of Chloride Ligands by 3,5-Dimethylpyrazolate. *Inorg. Chem.* **2012**, *51*, 7977−7992.
(51) Han, M.; Tian, Y.; Yuan, Z.; Zhu, L.; Ma, B. A Phosphorescent Molecular "Butterfly" That Undergoes a Photoinduced Structural Change Allowing Temperature Sensing and White Emission. *Angew. Chem., Int. Ed.* **2014**, *53*, 10908−10912.
(52) Zhou, C.; Yuan, L.; Yuan, Z.; Doyle, N. K.; Dilbeck, T.; Bahadur, D.; Ramakrishnan, S.; Dearden, A.; Huang, C.; Ma, B. Phosphorescent Molecular Butterflies with Controlled Potential-Energy Surfaces and Their Application as Luminescent Viscosity Sensor. *Inorg. Chem.* **2016**, *55*, 8564−8569.
(53) Lockard, J. V.; Rachford, A. A.; Smolentsev, G.; Stickrath, A. B.; Wang, X.; Zhang, X.; Atenkoffer, K.; Jennings, G.; Soldatov, A.; Rheingold, A. L.; et al. Triplet Excited State Distortions in a Pyrazolate Bridged Platinum Dimer Measured by X-Ray Transient Absorption Spectroscopy. *J. Phys. Chem. A* **2010**, *114*, 12780−12787.
(54) Cho, S.; Mara, M. W.; Wang, X.; Lockard, J. V.; Rachford, A. A.; Castellano, F. N.; Chen, L. X. Coherence in Metal−Metal-to-Ligand-Charge-Transfer Excited States of a Dimetallic Complex Investigated by Ultrafast Transient Absorption Anisotropy. *J. Phys. Chem. A* **2011**, *115*, 3990−3996.
(55) Brown-Xu, S. E.; Kelley, M. S. J.; Fransted, K. A.; Chakraborty, A.; Schatz, G. C.; Castellano, F. N.; Chen, L. X. Tunable Excited-State Properties and Dynamics as a Function of Pt−Pt Distance in Pyrazolate-Bridged Pt(II) Dimers. *J. Phys. Chem. A* **2016**, *120*, 543−550.
(56) Haldrup, K.; Dohn, A. O.; Shelby, M. L.; Mara, M. W.; Stickrath, A. B.; Harpham, M. R.; Huang, J.; Zhang, X.; Møller, K. B.; Chakraborty, A.; et al. Butterfly Deformation Modes in a Photoexcited Pyrazolate-Bridged Pt Complex Measured by Time-Resolved X-Ray Scattering in Solution. *J. Phys. Chem. A* **2016**, *120*, 7475−7483.
(57) Koshiyama, T.; Omura, A.; Kato, M. Redox-Controlled Luminescence of a Cyclometalated Dinuclear Platinum Complex Bridged with Pyridine-2-thiolate Ions. *Chem. Lett.* **2004**, *33*, 1386−1387.
(58) Yoshida, M.; Yashiro, N.; Shitama, H.; Kobayashi, A.; Kato, M. A Redox-Active Dinuclear Platinum Complex Exhibiting Multicolored Electrochromism and Luminescence. *Chem. - Eur. J.* **2016**, *22*, 491−495.
(59) Sicilia, V.; Borja, P.; Martín, A. Half-Lantern Pt(II) and Pt(III) Complexes. New Cyclometalated Platinum Derivatives. *Inorganics* **2014**, *2*, 508−523.
(60) Aoki, R.; Kobayashi, A.; Chang, H.-C.; Kato, M. Structures and Luminescence Properties of Cyclometalated Dinuclear Platinum(II) Complexes Bridged by Pyridinethiolate Ions. *Bull. Chem. Soc. Jpn.* **2011**, *84*, 218−225.
(61) Katlenok, E. A.; Zolotarev, A. A.; Ivanov, A. Y.; Smirnov, S. N.; Balashev, K. P. Structure, Optical and Electrochemical Properties of Binuclear Complexes with Platinated 2-Phenylbenzothiazol and Bridging 2-Mercapto-Derivatives of Pyridine, Pyrimidine, Benzothiazole, and Benzoxazole. *J. Struct. Chem.* **2015**, *56*, 880−886.
(62) Qi, X.; Djurovich, P. I.; Giebink, N. C.; Thompson, M. E.; Forrest, S. R. Evidence for Enhanced Dipolar Interactions between Pt Centers in Binuclear Phosphorescent Complexes. *Chem. Phys. Lett.* **2008**, *458*, 323−328.
(63) Kukushkin, V. Y.; Pombeiro, A. J. L.; Ferreira, C. M. P.; Elding, L. I. Dimethylsulfoxide Complexes of Platinum(II): K-[$PtCl_3(Me_2SO)$], Cis-[$PtCl_2L(Me_2SO)$] (L = Me_2SO, MeCN), [$PtCl(\mu$-Cl)(Me_2SO)](2), and [$Pt(Me_2SO)(4)$](CF_3SO_3)(2). *Inorg. Synth.* **2002**, *33*, 189−196.
(64) Brooks, J.; Babayan, Y.; Lamansky, S.; Djurovich, P. I.; Tsyba, I.; Bau, R.; Thompson, M. E. Synthesis and Characterization of Phosphorescent Cyclometalated Platinum Complexes. *Inorg. Chem.* **2002**, *41*, 3055−3066.
(65) Barboy, N.; Feitelson, J. Deoxygenation of Solutions for Transient Studies. *Anal. Biochem.* **1989**, *180*, 384−386.
(66) Suzuki, K.; Kobayashi, A.; Kaneko, S.; Takehira, K.; Yoshihara, T.; Ishida, H.; Shiina, Y.; Oishi, S.; Tobita, S. Reevaluation of Absolute Luminescence Quantum Yields of Standard Solutions Using a Spectrometer with an Integrating Sphere and a Back-Thinned CCD Detector. *Phys. Chem. Chem. Phys.* **2009**, *11*, 9850−9860.
(67) *SADABS*; Bruker-AXS Inc.: Madison WI, 2014.
(68) Sheldrick, G. M. A Short History of SHELX. *Acta Crystallogr., Sect. A: Found. Crystallogr.* **2008**, *64*, 112−122.
(69) Dolomanov, O. V.; Bourhis, L. J.; Gildea, R. J.; Howard, J. a. K.; Puschmann, H. OLEX2: A Complete Structure Solution, Refinement and Analysis Program. *J. Appl. Crystallogr.* **2009**, *42*, 339−341.
(70) Pavlishchuk, V. V.; Addison, A. W. Conversion Constants for Redox Potentials Measured versus Different Reference Electrodes in Acetonitrile Solutions at 25 °C. *Inorg. Chim. Acta* **2000**, *298*, 97−102.
(71) Frisch, M. J.; Trucks, G. W.; Schlegel, H. B.; Scuseria, G. E.; Robb, M. A.; Cheeseman, J. R.; Scalmani, G.; Barone, V.; Mennucci, B.; Petersson, G. A.; et al. *Gaussian 09*, revision D.01; Gaussian, Inc.: Wallingford, CT, 2009.
(72) Becke, A. D. A New Mixing of Hartree−Fock and Local Density-functional Theories. *J. Chem. Phys.* **1993**, *98*, 1372−1377.
(73) Becke, A. D. Density-functional Thermochemistry. III. The Role of Exact Exchange. *J. Chem. Phys.* **1993**, *98*, 5648−5652.
(74) Weigend, F.; Ahlrichs, R. Balanced Basis Sets of Split Valence, Triple Zeta Valence and Quadruple Zeta Valence Quality for H to Rn: Design and Assessment of Accuracy. *Phys. Chem. Chem. Phys.* **2005**, *7*, 3297−3305.
(75) Andrae, D.; Häußermann, U.; Dolg, M.; Stoll, H.; Preuß, H. Energy-adjusted *ab Initio* Pseudopotentials for the Second and Third Row Transition Elements. *Theor. Chim. Acta* **1990**, *77*, 123−141.
(76) Cossi, M.; Scalmani, G.; Rega, N.; Barone, V. New Developments in the Polarizable Continuum Model for Quantum Mechanical and Classical Calculations on Molecules in Solution. *J. Chem. Phys.* **2002**, *117*, 43−54.
(77) Dennington, R.; Keith, T.; Millam, J. *GaussView*, version 5; Semichem Inc.: Shawnee Mission, KS, 2009.
(78) Niehaus, T. A.; Hofbeck, T.; Yersin, H. Charge-Transfer Excited States in Phosphorescent Organo-Transition Metal Compounds: A Difficult Case for Time Dependent Density Functional Theory? *RSC Adv.* **2015**, *5*, 63318−63329.
(79) Kulikova, M. V.; Balashev, K. P.; Kvam, P. I.; Songstad, J. Effects of the Nature of the Ligand Environment and Metal Center on the Optical and Electrochemical Properties of Platinum(II) and Palladium-(II) Ethylenediamine Complexes with Heterocyclic Cyclometalated Ligands. *Russ. J. Gen. Chem.* **2000**, *70*, 163−170.
(80) Kvam, P.-I.; Puzyk, M. V.; Balashev, K. P.; Songstad, J.; Lundberg, C.; Arnarp, J.; Bjork, L.; Gawinecki, R. Spectroscopic and Electrochemical Properties of some Mixed-ligand Cyclometalated Platinum(II) Complexes Derived from 2-Phenylpyridine. *Acta Chem. Scand.* **1995**, *49*, 335−343.
(81) Jude, H.; Krause Bauer, J. A.; Connick, W. B. An Outer-Sphere Two-Electron Platinum Reagent. *J. Am. Chem. Soc.* **2003**, *125*, 3446−3447.
(82) Whittle, C. E.; Weinstein, J. A.; George, M. W.; Schanze, K. S. Photophysics of Diimine Platinum(II) Bis-Acetylide Complexes. *Inorg. Chem.* **2001**, *40*, 4053−4062.
(83) Pomestchenko, I. E.; Luman, C. R.; Hissler, M.; Ziessel, R.; Castellano, F. N. Room Temperature Phosphorescence from a Platinum(II) Diimine Bis(pyrenylacetylide) Complex. *Inorg. Chem.* **2003**, *42*, 1394−1396.
(84) Pomestchenko, I. E.; Castellano, F. N. Solvent Switching between Charge Transfer and Intraligand Excited States in a Multichromophoric Platinum(II) Complex. *J. Phys. Chem. A* **2004**, *108*, 3485−3492.
(85) Englman, R.; Jortner, J. The Energy Gap Law for Radiationless Transitions in Large Molecules. *Mol. Phys.* **1970**, *18*, 145−164.

DOI: 10.1021/acs.inorgchem.7b02736
Inorg. Chem. 2018, 57, 1298−1310

(86) Freed, K. F.; Jortner, J. Multiphonon Processes in the Nonradiative Decay of Large Molecules. *J. Chem. Phys.* **1970**, *52*, 6272−6291.
(87) Caspar, J. V.; Kober, E. M.; Sullivan, B. P.; Meyer, T. J. Application of the Energy Gap Law to the Decay of Charge-Transfer Excited States. *J. Am. Chem. Soc.* **1982**, *104*, 630−632.
(88) Caspar, J. V.; Meyer, T. J. Application of the Energy Gap Law to Nonradiative, Excited-State Decay. *J. Phys. Chem.* **1983**, *87*, 952−957.
(89) Kober, E. M.; Caspar, J. V.; Lumpkin, R. S.; Meyer, T. J. Application of the Energy Gap Law to Excited-State Decay of Osmium(II)-polypyridine Complexes: Calculation of Relative Nonradiative Decay Rates from Emission Spectral Profiles. *J. Phys. Chem.* **1986**, *90*, 3722−3734.
(90) Treadway, J. A.; Loeb, B.; Lopez, R.; Anderson, P. A.; Keene, F. R.; Meyer, T. J. Effect of Delocalization and Rigidity in the Acceptor Ligand on MLCT Excited-State Decay. *Inorg. Chem.* **1996**, *35*, 2242−2246.

DOI: 10.1021/acs.inorgchem.7b02736
Inorg. Chem. 2018, 57, 1298−1310